

Synthesis, crystal structures, luminescence, and photocatalytic properties of two 1D Co(II) coordination polymers constructed with semirigid bis(benzimidazole) and dicarboxylate ligands

Hai Ning Chang¹ · Yue Hua Li¹ · Zeng Chuan Hao¹ · Guang Hua Cui¹ 

Received: 14 July 2017 / Accepted: 11 September 2017 / Published online: 21 September 2017
© Springer International Publishing AG 2017

Abstract Two ternary cobalt(II) coordination polymers (CPs), namely $[\text{Co}(\text{L}1)(\text{nph})]_n$ (**1**) and $\{[\text{Co}_2(\text{L}2)_2(\text{nph})_2(\text{H}_2\text{O})] \cdot \text{H}_2\text{O}\}_n$ (**2**) (L1 = 4,4'-bis(benzimidazol-1-ylmethyl)biphenyl, L2 = 1,2-bis(5,6-dimethylbenzimidazol-1-ylmethyl)benzene, and H_2nph = 4-nitrophthalic acid) have been synthesized and structurally characterized by X-ray crystallography. Both CPs feature similar 1D infinite chains containing two distinct loops. CP **1** further forms a 3D supramolecular network via weak C–H...O hydrogen bond interactions. CP **2** shows a 1D two-layer chain structure, assembled through π – π stacking interactions. The electrochemical, luminescence, and photocatalytic activities of the two CPs for the removal of methylene blue under visible or UV light were investigated. Possible photocatalytic mechanisms are discussed.

Introduction

With the development of manufacturing industry, many toxic contaminants have been discharged into the water system [1–3]. Heterogeneous photocatalysis offers an environmentally friendly, inexpensive, and highly efficient

way to degrade such organic pollutants. Hence, research into coordination polymers (CPs) as functional materials has attracted considerable interest due to their high photocatalytic activities, tunable structures, and broad photoresponing range in the solar spectrum [4–7]. Although much progress has been made into the design and fabrication of CPs, it is still a challenge to predict the structures of the resultant frameworks. These crystalline architectures are influenced by several factors, including ligands, the preferred coordination environment of the metal nodes, pH of the reaction, temperature, solvent, and so on [8–12]. Hydrogen bonding and π – π stacking interactions can be used as structure-directing tools for the assembly of CPs and may also be used to link the low-dimensional entities into higher dimensionalities [13–15]. Therefore, the prospect of tuning the architectures and properties of CPs through modification of organic ligands provides an impetus for further research into supramolecular coordination polymers [16–18].

Semirigid bis(benzimidazole) derivatives having sp^3 hybridization of their $-\text{CH}_2-$ spacers can freely twist to meet the coordination requirements of different metal centers in the assembly process, resulting in CPs with robust networks and useful properties, as well as allowing for extended N-donor frameworks [19–21]. Meanwhile, aromatic dicarboxylate ligands such as phthalic acid, terephthalic acid, and isophthalic acid are frequently used to fabricate CPs, due to their versatile coordination modes and strong coordinating abilities. The effect of counter anions on the assembly of dicarboxylate and metal centers may be mitigated [22–24]. Structures and properties of target CPs are also affected by the electronic and steric characteristics of ligand substituents. In particular, dicarboxylate ligand substituents are often involved in

Electronic supplementary material The online version of this article (doi:10.1007/s11243-017-0186-0) contains supplementary material, which is available to authorized users.

✉ Guang Hua Cui
tscghua@126.com

¹ College of Chemical Engineering, Hebei Key Laboratory for Environment Photocatalytic and Electrochemical Materials, North China University of Science and Technology, No. 21 Bohai Road, Caofeidian New-City, Tangshan 063210, Hebei, People's Republic of China

supramolecular assemblies because of their particular ability to shape hydrogen bonding [25–27].

To further investigate the photocatalytic properties of bis(benzimidazole)-based ternary cobalt(II) coordination polymers [9], herein we report the syntheses and characterization of two cobalt(II) mixed CPs, namely $[\text{Co}(\text{L1})(\text{npht})]_n$ (**1**) and $\{[\text{Co}_2(\text{L2})_2(\text{npht})_2(\text{H}_2\text{O})]\cdot\text{H}_2\text{O}\}_n$ (**2**) (L1 = 4,4'-bis(benzimidazol-1-ylmethyl)biphenyl, H₂npht = 4-nitrophthalic acid, and L2 = 1,2-bis(5,6-dimethylbenzimidazol-1-ylmethyl)benzene). The resulting CP **1** and CP **2** materials possess narrow band gaps (E_g) and strong absorption in the visible and ultraviolet regions. The thermal analysis, luminescence properties and photocatalytic performances of CPs **1** and **2** for the degradation of methylene blue (MB) have been investigated.

Experimental

Materials and measurements

The proligands L1 and L2 were synthesized according to the previously reported procedure [28]. Other reagents were obtained from Jinan Henghua Sci. and Tec. Co. Ltd. and used without further purification. Elemental analysis for C, H, N was obtained on a Perkin-Elmer 240C elemental analyzer. Ultrasound was generated by a multiwave KQ2200DE instrument at a frequency of 40 kHz. The morphology and size of the samples before and after photodegradation of MB solutions were characterized with a scanning electron microscope (JSM-IT100) after gold coating. FTIR spectra (4000–400 cm^{-1}) were recorded on KBr disks on an Avatar 360 (Nicolet) spectrophotometer. Thermogravimetric analysis (TGA) was conducted on a Netzsch TG 209 thermal analyzer under N₂ with a heating rate of 10 °C min⁻¹. Powder X-ray diffraction (PXRD) patterns were measured on a Rigaku D/Max-2500 diffractometer with Cu-K α radiation ($\lambda = 1.5418 \text{ \AA}$). Luminescence spectra were collected with an FS5 fluorescence spectrophotometer at room temperature. Solid-state UV/Vis diffuse reflectance spectra were measured using a UV-Vis Puxi T9 UV-visible spectrophotometer, with BaSO₄ as a reflectance standard. The electrochemical analysis was carried out using a CHI 660E electrochemical workstation (Chenhua Instrument, Shanghai, China) in 0.1 M Na₂SO₄ electrolyte solution.

Synthesis of CP 1

A mixture of Co(OAc)₂·4H₂O (0.1 mmol, 24.8 mg), L1 (0.1 mmol, 36.6 mg), H₂npht (0.1 mmol, 21.1 mg), and H₂O (12 mL) was transferred to a 25 mL Teflon-lined stainless steel vessel and heated to 140 °C for 72 h. After

cooling to room temperature at a rate of 5 °C h⁻¹, pink block crystals were obtained by filtration and washed with distilled water. Yield (43.1 mg, 52.2%) based on Co. Elemental analysis (%) calcd for C₃₆H₂₅N₅CoO₆ (682.54): C, 63.4; H, 3.7; N, 10.3. Found (%): C, 63.6; H, 3.9; N, 10.5. IR (KBr, cm^{-1}): 2920(w), 1644(s), 1514(s), 1463(w), 1440(m), 1383(s), 1345(s), 1091(m), 780(w), 743(s).

Synthesis of CP 2

The synthesis of CP **2** was similar to that of CP **1**, except that L2 (0.1 mmol, 39.4 mg) was used in place of L1. Purple red block crystals of CP **2** were obtained. Yield (39.9 mg, 46.8%) based on Co. Elemental analysis (%) calcd for C₆₈H₆₂N₁₀Co₂O₁₄ (1361.16): C, 60.0; H, 4.6; N, 10.3. Found (%): C, 60.2; H, 4.8; N, 10.6. IR (KBr, cm^{-1}): 3445(s), 3110(w), 2920(w), 1624(s), 1515(s), 1442(s), 1210(w), 834(w), 622(w).

X-ray crystallography

Crystallographic diffraction data for CP **1** were collected on a Bruker Smart 1000 CCD diffractometer using graphite-monochromated Mo-K α radiation ($\lambda = 0.71073 \text{ \AA}$) with multiscan mode at 273(2) K. A semiempirical absorption correction was applied using the SADABS program [29]. Crystallographic data for CP **2** were collected at 100(2) K on an Agilent SuperNova Dual diffractometer with a Cu microfocus source and focusing multilayer optics. CrysAlis PRO software was used to collect, index, scale, and apply analytical absorption corrections based on faces of the crystal [30]. Both structures were refined on F^2 by full-matrix least squares techniques using the SHELXL-2014 program [31]. The ligands in the structure of CP **1** were severely disordered, such that atoms C35, O3, O4, N5, O5, O6; C29, C30, C31, C32, C33, C34 in the npht²⁻ ligand and atoms C16, C17, C18, C19 of the L1 ligand were refined using a split model. The corresponding site occupation factors were refined so that their sum was unity, 0.50/0.50, 0.44/0.56, 0.32/0.68, respectively. The corresponding bond distances in the disordered groups were restrained to be equal. The Uij parameters of these atoms were restrained to an approximate isotropic behavior. All non-hydrogen atoms were refined anisotropically. Hydrogen atoms of organic ligands were placed in calculated positions and included as riding atoms with isotropic displacement parameters. Residual hydrogen atoms of water molecules were located on a difference Fourier map. Crystallographic data and structure parameters for CP **1** and CP **2** are summarized in Table 1. Selected bond lengths and angles are listed in Table 2.

Table 1 Crystal and refinement data for CPs 1–2

	CP 1	CP 2
Empirical formula	C ₃₆ H ₂₅ N ₅ CoO ₆	C ₆₈ H ₆₂ Co ₂ N ₁₀ O ₁₄
Formula weight	682.54	1361.13
Temperature	273(2)	100(2)
Crystal system	Triclinic	Triclinic
Space group	<i>P</i> $\bar{1}$	<i>P</i> $\bar{1}$
<i>a</i> (Å)	10.6315(5)	12.5413(6)
<i>b</i> (Å)	12.0764(6)	12.9715(4)
<i>c</i> (Å)	12.8190(6)	19.6877(7)
α (°)	99.2180(10)	79.334(3)
β (°)	105.2200(10)	84.829(4)
γ (°)	97.3250(2)	76.834(4)
<i>V</i> (Å ³)	1542.56(13)	3060.9(2)
<i>Z</i>	2	2
<i>D</i> _{calc} (g/m ³)	1.469	1.477
μ (mm ⁻¹)	0.614	4.897
<i>F</i> (000)	702	1412
<i>R</i> _{int}	0.0351	0.0481
GOF	1.102	1.019
<i>R</i> ₁ (<i>I</i> > 2 σ (<i>I</i>))	0.0606	0.0602
<i>wR</i> ₂ (<i>I</i> > 2 σ (<i>I</i>))	0.1380	0.1588

Results and discussion

Crystal structure of CP 1

X-ray crystallographic analysis reveals that CP 1 crystallizes in the triclinic crystal system, space group *P* $\bar{1}$ with one Co(II) center, one L1 ligand, and one npht²⁻ ligand in the asymmetric unit. As depicted in Fig. 1a, the Co(II) center adopts a tetrahedral coordination geometry, of which the four vertexes are O1, O3A, N4, and N1B (symmetry codes: A: $-x + 2, -y + 1, -z + 2$; B: $-x + 1, -y + 2, -z + 1$). The two nitrogen and two oxygen atoms are provided by two L1 ligands and two npht²⁻ ligands, respectively. The Co–O/N bond lengths vary from 1.945(2) to 2.032(3) Å.

The L1 ligands adopt a *trans*-conformation, with N_{donor}–N–C_{sp3}–C_{sp3} torsion angles of 69.02(6)°. Each L1 ligand acts as a μ_2 -bridging linker, bridging adjacent Co centers to form a [Co₂(L1)₂] loop with a non-bonding Co...Co distance of 15.803(8) Å. The npht²⁻ ligands adopt a (κ^1)-(κ^0)-(κ^1)-(κ^0)- μ_2 coordination mode, connecting neighboring Co centers to generate a [Co₂(npht)₂] ring with a non-bonding Co...Co separation of about 5.300(6) Å. Two of these different loops cross-link each other to obtain a 1D chain (Fig. 1b). In addition, adjacent 1D loop-like chains are further extended into a 2D supramolecular architecture

Table 2 Selected bond lengths (Å) and angles (°) for CPs 1–2

CP 1			
Co1–O1	1.945(2)	Co1–O3A	1.970(3)
Co1–N1B	2.032(3)	Co1–N4	2.018(3)
O1–Co1–O3A	114.4(7)	O1–Co1–N1B	100.14(10)
O1–Co1–N4	108.56(10)	O3A–Co1–N1B	117.2(7)
O3A–Co1–N4	105.2(8)	N4–Co1–N1B	111.26(11)
CP 2			
Co1–O1	2.025(2)	Co1–N10A	2.080(3)
Co1–N3	2.093(3)	Co1–O7	2.164(2)
Co1–O1W	2.196(2)	Co1–O8	2.209(2)
Co2–O3	2.006(2)	Co2–O10	2.027(2)
Co2–N7	2.029(2)	Co2–N6B	2.089(3)
O1–Co1–N10A	104.15(10)	O1–Co1–N3	90.76(10)
N10A–Co1–N3	93.27(10)	O1–Co1–O7	159.56(9)
N10A–Co1–O7	95.22(10)	N3–Co1–O7	94.64(10)
O1–Co1–O1W	90.28(9)	N10A–Co1–O1W	88.09(9)
N3–Co1–O1W	178.04(10)	O7–Co1–O1W	83.82(9)
O1–Co1–O8	99.39(9)	N10A–Co1–O8	155.57(10)
N3–Co1–O8	92.85(9)	O7–Co1–O8	60.70(8)
O1W–Co1–O8	85.34(8)	O3–Co2–O10	106.51(9)
O3–Co2–N7	119.40(10)	O10–Co2–N7	113.73(10)
O3–Co2–N6B	116.78(10)	O10–Co2–N6B	98.10(10)
N7–Co2–N6B	100.49(10)		

Symmetry codes for CP 1: A: $-x + 2, -y + 1, -z + 2$; B: $-x + 1, -y + 2, -z + 1$; for CP 2: A: $x + 1, y - 1, z$; B: $x - 1, y + 1, z$

through C5–H5...O2C hydrogen bonding interactions between the L1 ligands and npht²⁻ ligands (H5...O2 = 2.36 Å, C5–H5...O2 = 149°, symmetry code: C = $x + 1, y, z$; Fig. 1c). In addition, the 2D structure is further extended into a 3D supramolecular framework via C17–H17...O2D hydrogen bonding interactions between L1 and npht²⁻ ligands (H17...O2 = 2.50 Å, C17–H17...O2 = 148°, symmetry code: D = $-x, -y + 1, -z + 1$; Fig. 1d).

Crystal structure of CP 2

CP 2 crystallizes in the triclinic space group *P* $\bar{1}$. The asymmetric unit comprises two individual Co(II) centers, two npht²⁻ ligands, two L2 ligands, one-coordinated water ligand, and one lattice water molecule. As illustrated in Fig. 2a, the Co1 center is six-coordinated by two nitrogen atoms (N3, N10A, symmetry codes: A: $x + 1, y - 1, z$) from two L2 ligands, plus four oxygen atoms (O1, O7, O8, O1W) from the carboxyl groups of two npht²⁻ ligands and one water molecule, giving a distorted octahedral geometry. Dissimilar to Co1, the Co2 center is four-coordinated

Fig. 1 **a** Coordination environment of Co(II) centers in CP **1** with 30% thermal ellipsoids. Hydrogen atoms are omitted for clarity (symmetry codes: A: $-x + 2, -y + 1, -z + 2$; B: $-x + 1, -y + 2, -z + 1$). **b** The 1D chain structure in CP **1**. **c** The 2D supramolecular architecture extended through C5–H5...O2C hydrogen bonding interactions (bright green dashed line, symmetry codes: C: $x + 1, y, z; -x + 2, -y + 1, -z + 2$). **d** The 3D supramolecular architecture further extended by C17–H17...O2D hydrogen bonding interactions (bright yellow dashed line, symmetry codes: D: $-x, -y + 1, -z + 1$)

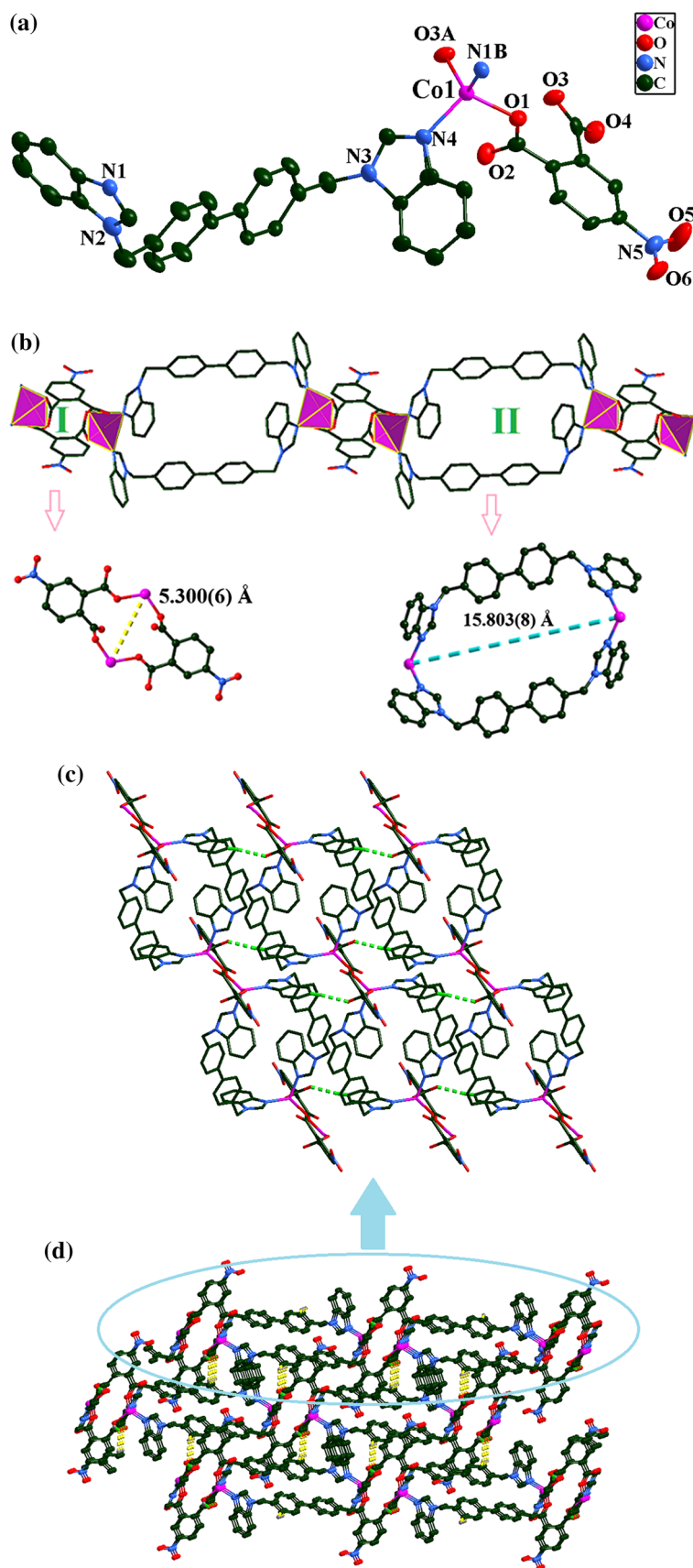
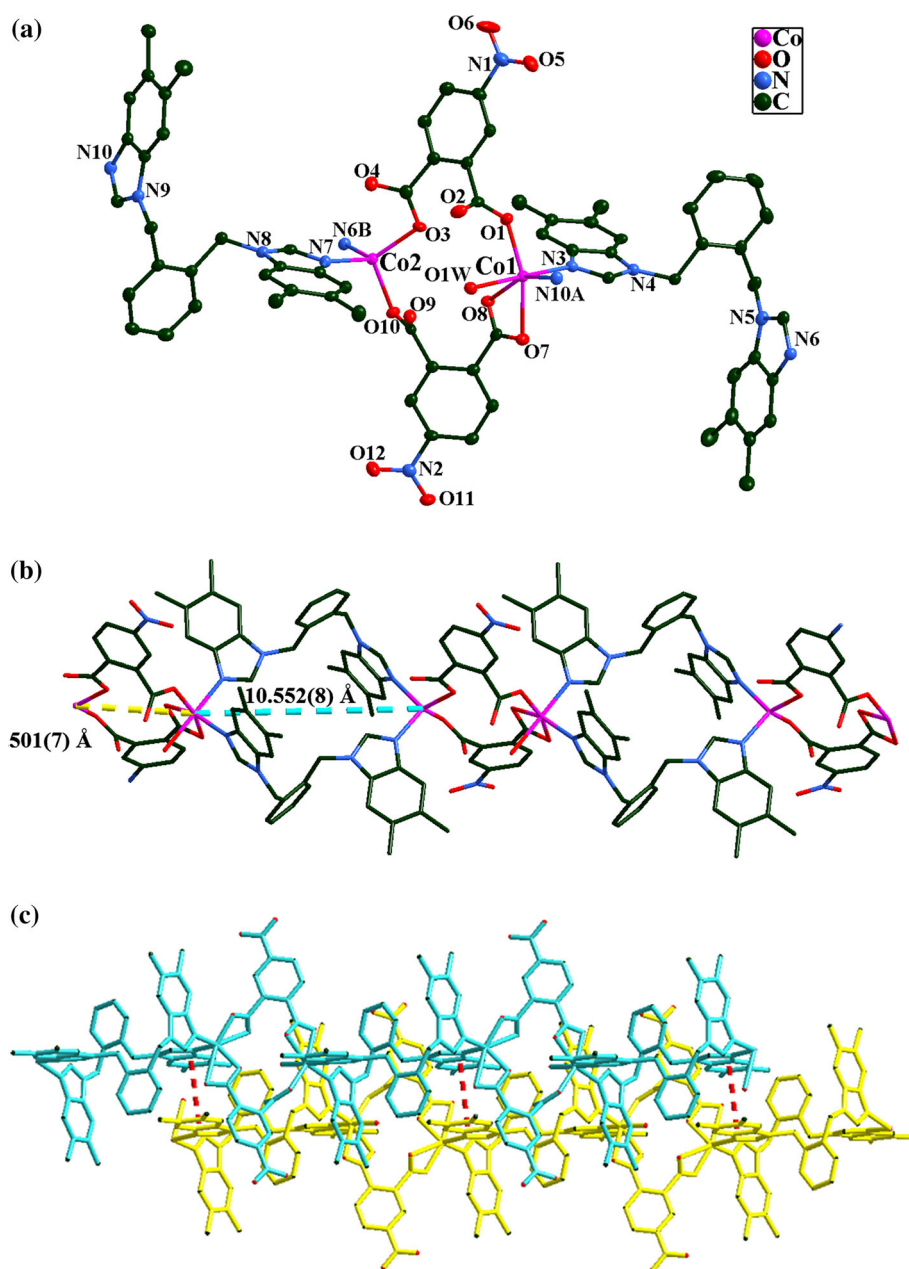


Fig. 2 **a** Coordination environment of Co(II) centers in CP 2 with 30% thermal ellipsoids. Hydrogen atoms and the free water molecule are omitted for clarity (symmetry codes: A: $-x + 2, -y + 1, -z + 2$; B: $-x + 1, -y + 2, -z + 1$). **b** View of the 1D loop-like chain in CP2. **c** 1D two-layer chain formed by π - π stacking interactions



by two oxygen atoms (O3, O10) of two independent npht^{2-} ligands and two nitrogen atoms (N6B, N7, symmetry codes: B: $x - 1, y + 1, z$) of two L2 ligands, in a distorted tetrahedral environment.

As shown in Fig. 2b, two distinct L2 ligands serve as bridges linking pairs of Co(II) centers to build a rectangular $[\text{Co}_2(\text{L2})_2]$ ring, in which the dihedral angles between the mean planes of the two benzimidazole rings of the two L2 ligands are $85.72(6)^\circ$ and $86.94(6)^\circ$, and the $\text{Co1}\cdots\text{Co2}$ distance is $10.552(8)$ Å. The npht^{2-} ligands show two coordination modes, specifically $(\kappa^1)-(\kappa^0)-(\kappa^1)-(\kappa^0)-\mu_2$ and $(\kappa^1)-(\kappa^1)-(\kappa^1)-(\kappa^0)-\mu_2$, and connect adjacent Co(II) centers

to shape another $[\text{Co}_2(\text{npht})_2]$ loop, with a $\text{Co1}\cdots\text{Co2}$ distance of $5.501(7)$ Å. The neighboring two loops are further cross-linked with each other to generate a 1D chain. In addition, through π - π stacking interactions between the benzene rings of two L2 ligands (centroid-to-centroid distance of 3.752 Å, interplanar angle α , slipping angles β and γ of 0° , 17.78° and 17.78° , respectively; Cg1: C44–C45–C46–C47–C48–C49, Cg1C: C44C–C45C–C46C–C47C–C48C–C49C, symmetry codes: C = $-x, -y + 1, -z + 1$; Fig. 2c), these 1D loop-like chains are extended into a 1D two-layer chain structure, which is further consolidated by $\text{O2W}\cdots\text{H2WA}\cdots\text{O10D}$ hydrogen bonding

interactions between water ligands and nph^{2-} ligands ($\text{H2WA}\cdots\text{O10} = 2.14 \text{ \AA}$, $\text{O2W-H2WA}\cdots\text{O10D} = 151^\circ$, symmetry code: $D = x, y + 1, z$).

In comparison with the present work, two related coordination polymers have been reported previously, namely $\{[\text{Co}(\text{L1})(1,3\text{-bdc})(\text{H}_2\text{O})]\cdot 1.5\text{H}_2\text{O}\}_n$ (**3**) and $\{[\text{Co}_2(\text{L1})_2(\text{nip})_2]\cdot 2\text{H}_2\text{O}\}_n$ (**4**) (1,3-H₂bdc = 1,3-benzenedicarboxylic acid and H₂nip = 5-nitroisophthalic acid) [32]. Thus, two semirigid bis(benzimidazole) derivatives (L1 and L2) with different spacers gave four cobalt(II) CPs. CP **1** and CP **2** exhibit 1D chain structures, while CP **3** and CP **4** are 2D layered frameworks. In four complexes, the N-donor ligands all adopt the bidentate bridging mode, linking the Co(II) centers with Co \cdots Co separations of 15.803(8) Å for CP **1**, 10.552(8) Å for CP **2**, 17.921 Å for CP **3**, and 13.803 and 16.778 Å for CP **4**. The four Co(II) centers show different coordination geometries (tetrahedral for CP **1**, distorted octahedral and tetrahedral for CP **2**, distorted octahedral for CP **3** and CP **4**, Tables 3 and 4). In CP **1**, the nph^{2-} ligand adopts the bis-monodentate coordination mode, while the nph^{2-} ligands employ the bis-monodentate and chelating-monodentate coordination modes for CP **2**. Further, the 1,3-bdc²⁻ ligands of CP **3** adopt a bidentate–monodentate

coordination mode to act as connectors in a 2D 4-connected ($4^4,6^2$) **sql** net, while the nip^{2-} ligands of CP **4** exhibit bis-bidentate coordination, resulting in a 2D uninodal 4-connected ($4^3.6^3$) network. Finally, CP **1** and CP **4** are self-assembled into 3D supramolecular structures via hydrogen bonding interactions, while CP **2** is further formed into a 1D bilayer chain through π – π stacking interactions. Overall, the different dimensionalities of CPs **1–4** may be attributed to their different aromatic carboxylates and the resulting supramolecular interactions.

Infrared spectra, PXRD and TGA

The IR spectra of CP **1** and CP **2**, respectively, show characteristic absorption bands at 1644 and 1383 cm^{-1} for CP **1**, 1624 and 1442 cm^{-1} for CP **2**, attributed to the asymmetric and symmetric stretching vibrations of the carboxylic groups. The benzimidazole $\nu_{(\text{C-N})}$ structures are observed at 1514 and 1515 cm^{-1} for CP **1** and CP **2**, respectively (Fig. S1). Powder X-ray diffraction (PXRD) experiments were carried out to confirm the phase purities of the bulk samples. The experimental PXRD patterns well matched the simulations, confirming the phase purity of the bulk samples (Fig. S2).

Table 3 Coordination modes of nph^{2-} , L1, and L2 ligands of CPs **1–2**

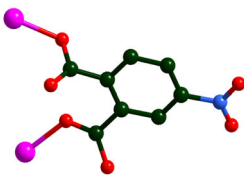
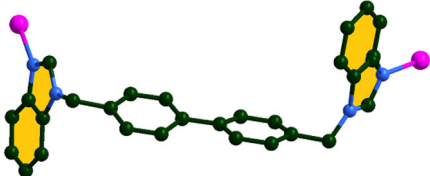
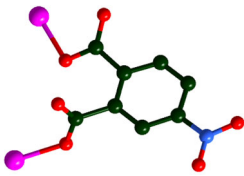
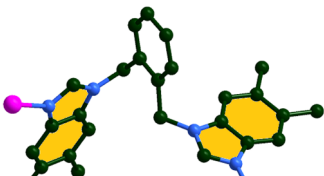
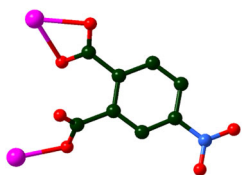
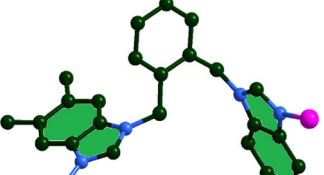
CPs	nph^{2-} ligand	N-donor ligands
CP 1		
CP 2		
		

Table 4 Comparison of the related complex of CPs 1–4

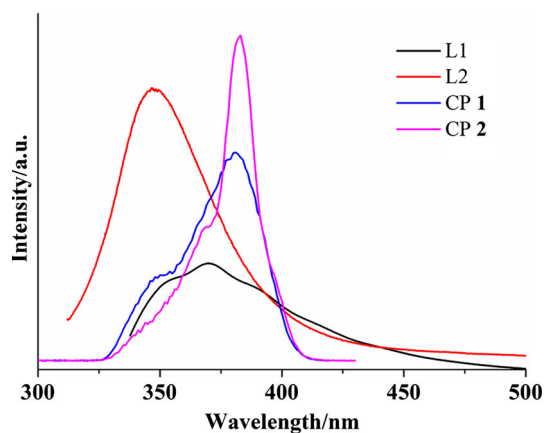
Related coordination polymers	Coordination number	Crystal structure	Dyes/catalytic efficiency	References
[Co(L1)(npht)] _n (1)	4	1D chain structure	MB/90.0%	This work
{[Co ₂ (L2) ₂ (npht) ₂ (H ₂ O)]·H ₂ O} _n (2)	4, 6	1D chain structure	MB/93.8%	This work
{[Co(L1)(1,3-bdc)(H ₂ O)]·1.5H ₂ O} _n (3)	6	2D (4,4) network	MO/91.1%	[32]
{[Co ₂ (L1) ₂ (nip) ₂]·2H ₂ O} _n (4)	6	2D framework	MO/96.8%	[32]

Where H₂npht = 4-nitrophthalic acid, 1,3-H₂bdc = 1,3-benzenedicarboxylic acid, H₂nip = 5-nitroisophthalic acid L1 = 4,4'-bis(benzimidazol-1-ylmethyl)biphenyl, and L2 = 1,2-bis(5,6-dimethylbenzimidazol-1-ylmethyl)benzene

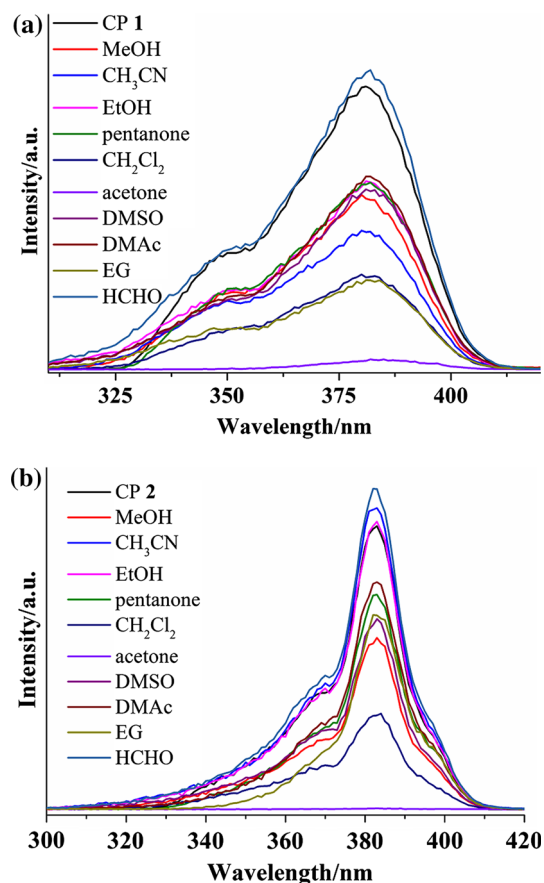
The TGA curve of CP **1** shows an initial weight loss above 185 °C, assigned to decomposition of the organic ligands. The residue corresponds to CoO (11.2% obsd; 11.0% calcd). For CP **2**, the TGA curve shows an initial weight loss of 2.5% from 130 to 225 °C, which is in good agreement with the removal of two water molecules (calcd. 2.6%). The second sharp weight loss is observed from 260 to 720 °C corresponding to decomposition of the organic ligands. The remaining residue of 5.7% corresponds to the formation of CoO (calcd 5.5%) (Fig. S3).

Luminescence properties

The luminescence spectra of both CPs and their corresponding free ligands were recorded in the solid state (Fig. 3). The proligands L1 and L2 show emission peaks at 370 nm ($\lambda_{\text{ex}} = 325$ nm) and 347 nm ($\lambda_{\text{ex}} = 300$ nm), respectively, which may be ascribed to $\pi \rightarrow \pi^*$ and/or $n \rightarrow \pi^*$ transitions [33, 34]. CPs **1** and **2** give luminescence emissions bands at 381 nm ($\lambda_{\text{ex}} = 304$ nm) and 383 nm ($\lambda_{\text{ex}} = 290$ nm), respectively, which show different degrees of redshift compared with the free proligands (ca. 11 nm for CP **1** and ca. 36 nm for CP **2**). These redshifts may be related to intraligand luminescence emissions [35].

**Fig. 3** Luminescence spectra of CPs 1–2, free ligands L1 and L2

In order to investigate the potential of the two CPs for sensing organic solvent molecules, 3 mg of the powder of CP (**1** or **2**) was immersed in 3 mL of organic solvent, specially methanol, acetonitrile, ethanol, pentanone, dichloromethane, acetone, DMSO, dimethylacetamide (DMAc), ethylene glycol (EG), and formaldehyde. Each suspension was treated by ultrasonication for 1.0 h. After aging for over 24 h, shaking, filtering, and drying in air, the corresponding fluorescence emission spectra were recorded at room temperature, with the results shown in Fig. 4. It is

**Fig. 4** Solid-state luminescence spectra of CP **1** (a) and CP **2** (b) after immersing the as-synthesized powders into various pure solvents

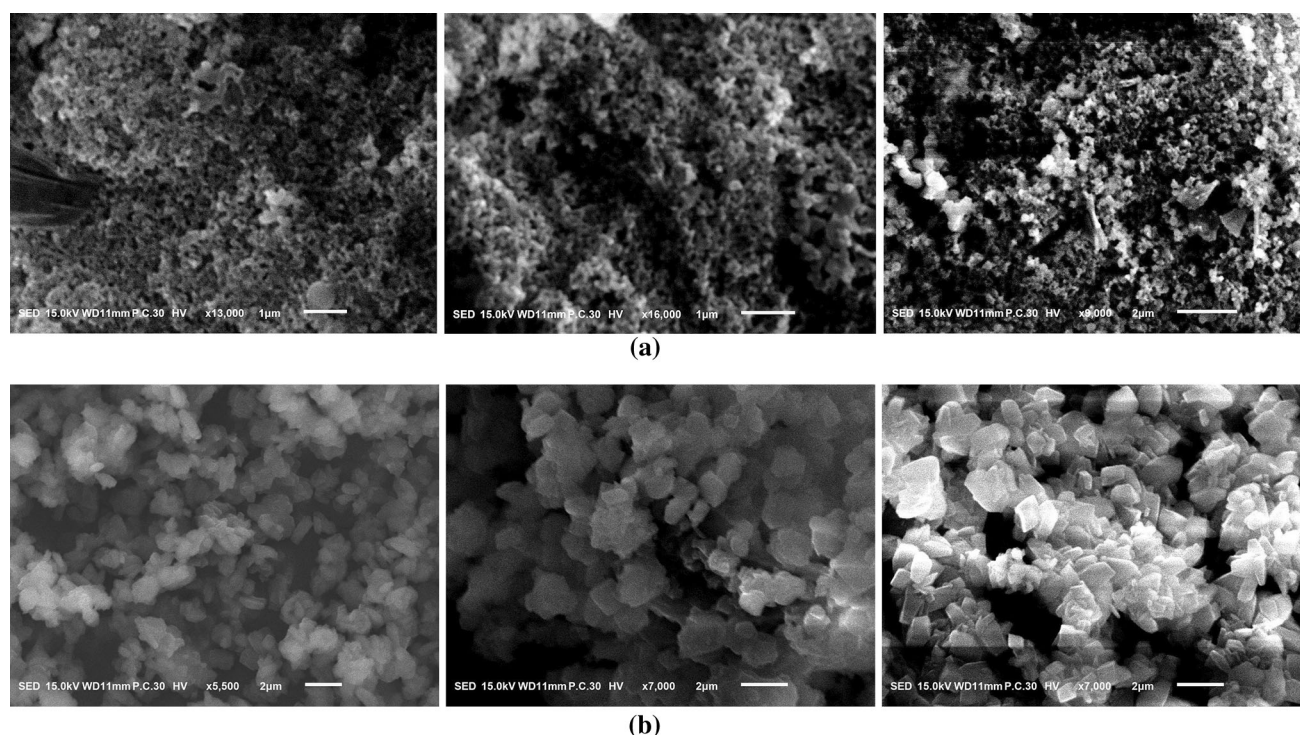


Fig. 5 **a** SEM images of nanopore structures of CP **1** (left), CP **1**@Acetone (middle), and CP **1** after the photodegradation of MB solutions under UV light irradiation (right). **b** SEM images of

cubelike nanostructures of CP **2** (left), CP **2**@Acetone (middle), and CP **2** after the photodegradation of MB solutions under UV light irradiation (right)

clear that only the luminescence intensity of CP **1**@HCHO was slightly enhanced. For the other CP **1**@solvents, different degrees of decreased luminescence were observed. In particular, acetone shows a significant quenching effect. For CP **2**, only the luminescence intensity of CP **2**@HCHO and CP **2**@CH₃CN was slightly enhanced; the other CP **2**@solvents showed decreases in luminescence, especially CP **2**@Acetone. In addition, the measured PXRD patterns of CP **1**@Acetone and CP **2**@Acetone well matched the corresponding simulated patterns, and the SEM images of CP **1**@Acetone and CP **2**@Acetone are similar to those of pure CP **1** and CP **2** powders, indicating that the structures of both CPs are well preserved (Figs. 5 and S2). Hence, both CP **1** and CP **2** can serve as potential luminescence sensors for detecting acetone.

Electrochemical behaviors

A method of preparation of CP bulk-modified carbon paste electrodes (CPE) is given in a previous paper [19]. To study the redox properties of the present CPs, the electrochemical properties of **1**-CPE and **2**-CPE were investigated in 0.1 M Na₂SO₄ at room temperature. As shown in Fig. 6, compared to the bare CPE, both **1**-CPE and **2**-CPE showed one quasireversible redox peak, such that the mean peak potential $E_{1/2} = (E_{pa} + E_{pc})/2$ was approximately 390 mV

for **1**-CPE and 386 mV for **2**-CPE; these can be attributed to the Co^{III}/Co^{II} redox couple [36]. The influence of varying scan rates on the electrochemical activities of **1**-CPE and **2**-CPE was also studied. As depicted in Fig. 6, the peak potentials changed gradually: the cathodic peak potentials shifted to negative direction and the corresponding anodic peak potentials shifted to positive direction. The anodic and cathodic peak currents are proportional to the scan rates, suggesting that the redox processes are close to being surface-controlled for both CPEs [37].

Photocatalytic activities

The UV/Vis diffuse reflectance spectra were recorded in order to obtain the band gaps (E_g) of the two CPs [38, 39]. As depicted in Fig. 7a, CP **1** and CP **2** exhibit intense absorption bands at 260 and 320 nm, respectively, which can be attributed to $\pi^* \rightarrow \pi$ or $\pi^* \rightarrow n$ transitions of the ligand or metal-to-ligand charge transfer. An additional broad adsorption band in the visible region for both CPs may originate from the $d \rightarrow d$ spin-allowed transition of the Co(II) centers [40]. The band gaps (E_g) were determined as the intersection point between the energy axis and the line extrapolated from the linear portion of the absorption edge in a plot of Kubelka–Munk function F versus energy E . The Kubelka–Munk function is given by:

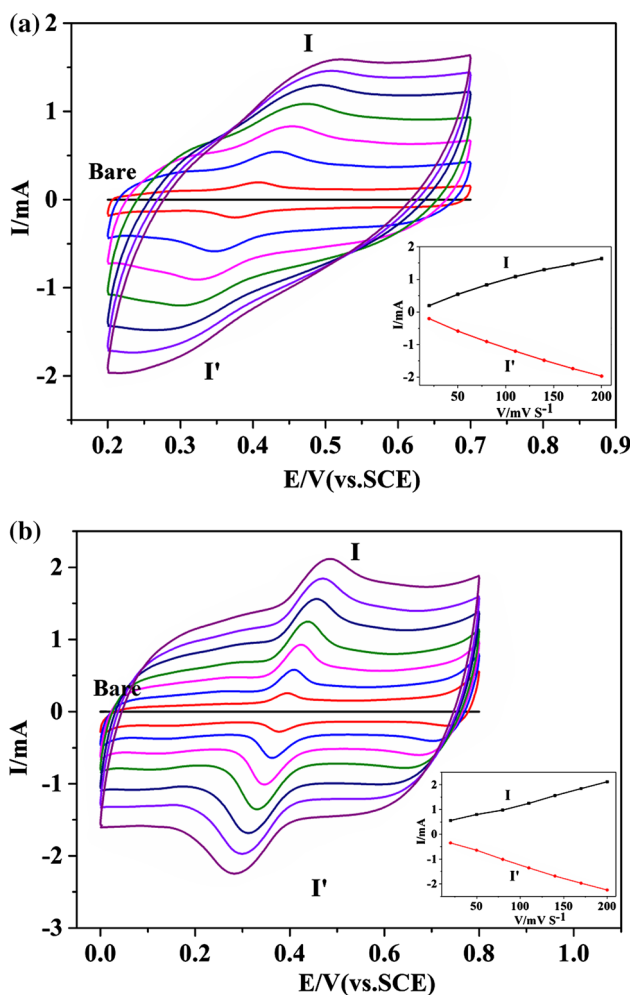


Fig. 6 Cyclic voltammograms of 1-CPE and 2-CPE at different scan rates (from inner to outer): 20, 50, 80, 110, 140, 170, 200 mV s^{-1} in 0.1 M Na_2SO_4 aqueous solution. The inset shows the plots of the anodic and the cathodic peak currents versus scan rates

$$F = (1 - R)^2 / 2R \tag{1}$$

where R is the reflectance of an infinitely thick layer at a given wavelength. Plots of F versus E for both CPs are shown in Fig. 7b, and E_g values for CP 1 and CP 2 were obtained as 2.9 and 2.8 eV, respectively.

Photocatalytic experiments for the degradation of methylene blue (MB) were carried out, and the detailed reaction process is given in the supporting information. The photodegradation of MB without any catalyst was investigated under the same conditions, as a control experiment. As shown in Figs. 8 and S4, the photodegradation efficiency of the control experiment under UV irradiation was only 13.9% after 105 min. CP 1 showed significant catalytic behavior, with photodegradation efficiencies of 55.4 and 90.0% under visible and UV light irradiations, respectively. Similarly, CP 2 also exhibited good catalytic behavior, with photodegradation efficiencies of 56.9 and

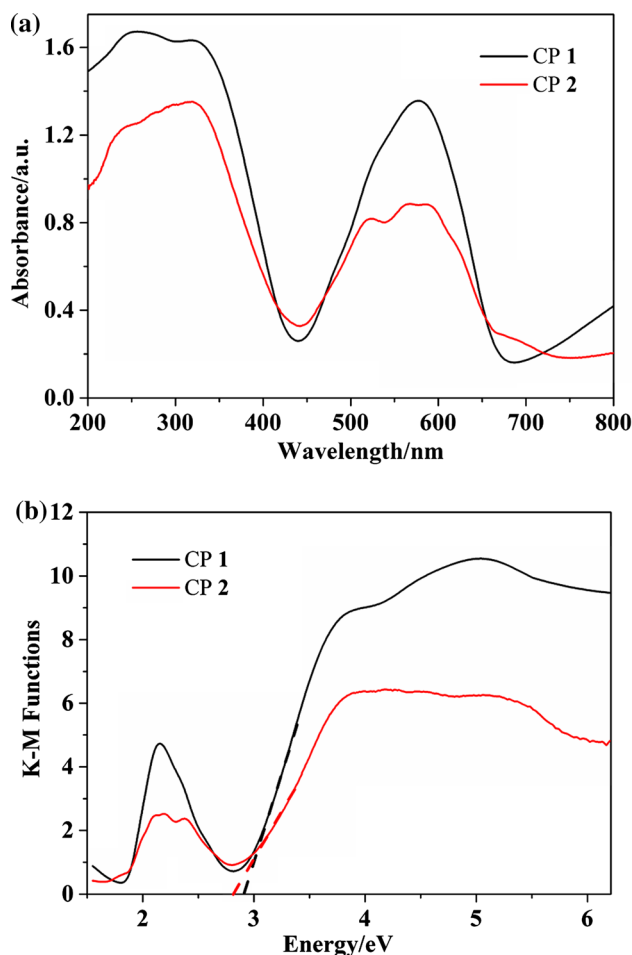


Fig. 7 a UV-vis absorption spectra of CP 1 and CP 2. b Diffuse reflectance spectra of Kubelka–Munk functions versus energy (eV) for CP 1 and CP 2

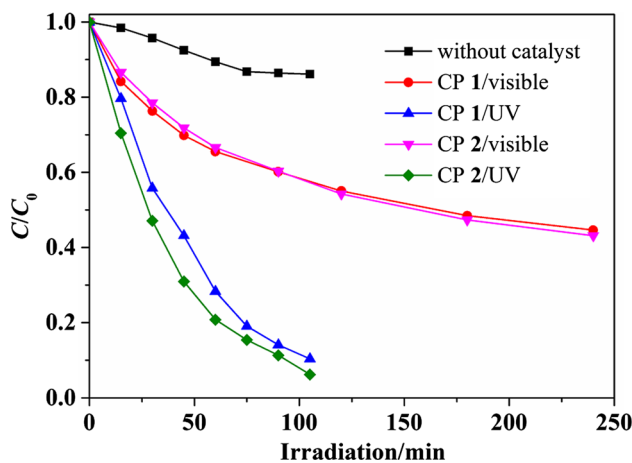


Fig. 8 Experimental results of the photocatalytic degradation of methyl blue

93.8% under visible/UV light irradiations, respectively. Hence, both CPs are promising candidates for the degradation of dyes, especially under UV irradiation. The

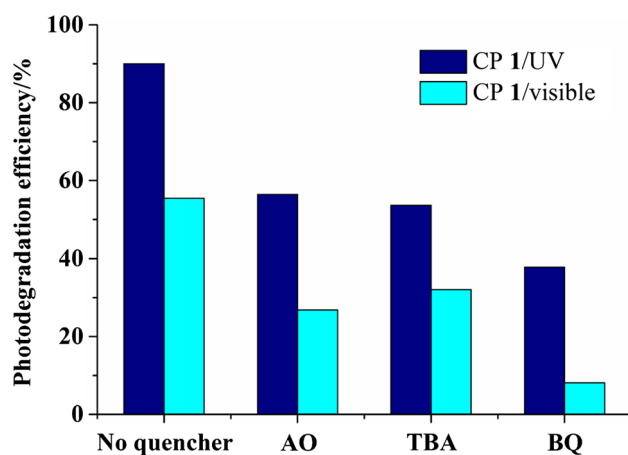


Fig. 9 Trapping experiment of active species during the photocatalytic reaction for CP 1

slightly different catalytic behaviors of the two CPs may be due to the different coordination environments about the Co(II) centers [41]. However, the previously described CPs 3 and 4 showed higher photocatalytic activities than CPs 1 and 2 under UV irradiation (Table 4).

To verify the possible photocatalytic reaction mechanism, trapping experiments for the active species of both CPs were conducted in the presence of tertiary butyl alcohol (TBA, a quencher of $\cdot\text{OH}$), benzoquinone (BQ, a quencher of $\cdot\text{O}_2^-$), and ammonium oxalate (AO, a quencher of holes, h^+). As shown in Fig. 9 and Fig. S5, the photodegradation of MB was affected by the addition of TBA, BQ, and AO; BQ in particular had the most significant effect on the photocatalytic removal of MB by both CPs. These observations suggest that among the photo-generated species $\cdot\text{O}_2^-$, h^+ and $\cdot\text{OH}$, the $\cdot\text{O}_2^-$ radical is the main active species in these experiments [42].

Accordingly, a possible photocatalytic reaction mechanism for two CPs may be deduced. Under light irradiation, L1, L2, and/or the H_2npht ligands encourage N and/or O to Co center charge transfer and it promote electrons from the HOMO to the LUMO. This concomitantly results in the same amount of holes (h^+). The hydroxyl radical ($\cdot\text{OH}$) is then generated by the combination of H^+ with $\cdot\text{O}_2^-$ generated from the reduction of O_2 by e^- . In order for the CP to return to its stable HOMO state, one electron is captured from water, resulting in the formation of $\cdot\text{OH}$ radicals. These $\cdot\text{OH}$ active species can efficiently decompose the MB, giving the photocatalytic effect.

In addition, successive cycle experiments have been carried out, as shown in Fig. S6. The photodegradation efficiencies of both CPs as catalysts show no obvious decline over several experiments. PXRD and SEM images of both CPs were recorded after the photocatalytic reactions (Figs. 5 and S2). The PXRD patterns are nearly

identical to those of the original CPs, while the SEM images indicate that the surfaces of the CPs before and after photocatalysis were quite similar. Hence, both CP 1 and CP 2 possess good stability toward photocatalysis and may be used repeatedly.

Conclusion

Two Co(II) coordination polymers based on semirigid bis(benzimidazole) ligands have been synthesized and characterized. CP 1 exhibits a 1D chain structure, further extended into a 3D supramolecular framework through C–H \cdots O hydrogen bonding interactions, while CP 2 also shows a 1D loop-like chain, with a bilayer structure formed by π – π stacking interactions. Both of these CPs act as selective fluorescent sensors for acetone and also show photocatalytic behaviors for the decomposition of MB solutions under visible or UV light irradiation, although their efficiencies are lower than those of some related CPs, which were reported previously.

Supplementary materials

CCDC 1560789 and 1561077 contain the supplementary crystallographic data for CPs 1–2. These data can be obtained free of charge via <http://www.ccdc.cam.ac.uk/conts/retrieving.html>, or from the Cambridge Crystallographic Data Centre, 12 Union Road, Cambridge CB21EZ, UK; fax: (+44) 1223-336-033; or e-mail: deposit@ccdc.cam.ac.uk.

Acknowledgements The project was supported by the National Natural Science Foundation of China (51474086), Natural Science Foundation – Steel and Iron Foundation of Hebei Province (B2015209299).

References

1. Wan Z, Zhang G, Wu XY, Yin S (2017) *Appl Catal B* 207:17–26
2. Sun M, Wang Y, Shao Y, He YH, Zeng Q, Liang HK, Yan T, Du B (2017) *J Colloid Interface Sci* 501:123–132
3. Ghanbari F, Moradi M (2017) *Chem Eng J* 310:41–62
4. Zhang JW, Kan XM, Li XL, Luan J, Wang XL (2015) *CrystEngComm* 17:3887–3907
5. Wu XY, Qi HX, Ning JJ, Wang JF, Ren ZG, Lang JP (2015) *Appl Catal B* 168:98–104
6. Meng W, Xu ZQ, Ding J, Wu DQ, Han X, Hou HW, Fan YT (2014) *Cryst Growth Des* 14:730–738
7. Chen YQ, Li GR, Qu YK, Zhang YH, He KH, Gao Q, Bu XH (2013) *Cryst Growth Des* 13:901–907
8. Zhou HF, He T, Yue KF, Liu YL, Zhou CS, Yan N, Wang YY (2016) *Cryst Growth Des* 16:3961–3968
9. Hao SY, Hou SX, Van Hecke K, Cui GH (2017) *Dalton Trans* 47:1951–1964

10. Cui JW, An WJ, Van Hecke K, Cui GH (2016) *Dalton Trans* 45:17474–17484
11. Nath JK, Mondal A, Powell AK, Baruah JB (2014) *Cryst Growth Des* 14:4735–4748
12. Kang YF, Liu JQ, Liu B, Zhang WT, Liu Q, Liu P, Wang YY (2014) *Cryst Growth Des* 14:5466–5476
13. Li SB, Ma HY, Pang HJ, Zhang L (2014) *Cryst Growth Des* 14:4450–4460
14. Nobakht V, Beheshti A, Proserpio DM, Carlucci L, Abrahams CT (2014) *Inorg Chim Acta* 414:217–225
15. Wang X, Zhang J, Liu G, Lin H (2011) *J Solid State Chem* 184:280–288
16. Li X, Zhou P, Dong Y, Liu H (2015) *J Inorg Organomet Polym Mater* 4:650–656
17. Zhang MD, Qin L, Yang HT, Li YZ, Guo ZJ, Zheng HG (2013) *Cryst Growth Des* 13:1961–1969
18. Erer H, Yeşilel OZ, Arıcı M (2015) *Cryst Growth Des* 15:3201–3211
19. Wang XL, Le M, Lin HY, Luan J, Liu GC, Sui FF, Chang ZH (2015) *Inorg Chem Front* 2:373–387
20. He X, Lu XP, Li MX, Morris RE (2013) *Cryst Growth Des* 13:1649–1654
21. Liu L, Ding J, Li M, Lv XF, Wu J, Hou HW, Fan YT (2014) *Dalton Trans* 43:12790–12799
22. Shen Y, Fan CC, Wei YZ, Du J, Zhu HB, Zhao Y (2016) *Cryst Growth Des* 16:5859–5868
23. Wang XL, Gao Q, Liu GC, Lin HY, Tian AX, Li J (2011) *Inorg Chem Commun* 14:745–748
24. Liu L, Huang C, Xue X, Li M, Hou H, Fan Y (2015) *Cryst Growth Des* 15:4507–4517
25. Du M, Zhang ZH, You YP, Zhao XJ (2008) *CrystEngComm* 10:306–321
26. Abourahma H, Moulton B, Kravtsov V, Zaworotko MJ (2002) *J Am Chem Soc* 124:9990–9991
27. Abourahma H, Coleman AW, Moulton B, Rather B, Shahgaldian P, Zaworotko MJ (2001) *Chem Commun* 22:2380–2381
28. Li LL, Li HX, Ren ZG, Liu D, Chen Y, Zhang Y, Lang JP (2009) *Dalton Trans* 40:8567–8573
29. Sheldrick GM (1996) SADABS. University of Göttingen, Göttingen
30. Pro CA (2012) Data collection and data reduction software package. Agilent Technologies, Santa Clara
31. Sheldrick GM (2015) *Acta Crystallogr Sect C* 71:3–8
32. Hu JM, Guo R, Liu YG, Cui GH (2016) *Inorg Chim Acta* 450:418–425
33. Zhang X, Hou L, Liu B, Cui L, Wang YY, Wu B (2013) *Cryst Growth Des* 13:3177–3187
34. Yang YQ, Yang J, Kan WQ, Yang Y, Guo J, Ma JF (2013) *Eur J Inorg Chem* 2013:280–292
35. Pu AT, Yang J, Kan WQ, Yang Y, Ma JF (2013) *Polyhedron* 50:556–570
36. Hu JM, Blatov VA, Yu BY, Van Hecke K, Cui GH (2016) *Dalton Trans* 45:2426–2429
37. Cui GH, He CH, Jiao CH, Geng JC, Blatov VA (2012) *Crys-tEngComm* 14:4210–4216
38. Wen LL, Zhao JB, Lv KL, Wu YH, Deng KJ, Leng XK, Li DF (2012) *Cryst Growth Des* 12:1603–1612
39. Huan DH, Zhao YQ, Hao ZC, Cui GH (2016) *Z Anorg Allg Chem* 642:804–811
40. Sarma D, Ramanujachary KV, Lofland SE, Magdaleno T, Natarajan S (2009) *Inorg Chem* 48:11660–11676
41. Zhang X, Zhao YQ, Wang FS, Dong GY (2016) *Chin J Struct Chem* 35:765–773
42. Yu C, Li G, Kumar S, Yang K, Jin R (2014) *Adv Mater* 26:892–898